# ELECTRICAL DISCHARGE IN SUPERCRITICAL METHANOL

## S. B. LEONOV[1]*

[1] The Ohio State University, Dept of MAE, N350, 201 W. 19th Ave, Columbus, OH, 43210, USA
*leonov.2@osu.edu

## ABSTRACT

This paper presents results of an initial study of dynamics and properties of electrical discharge in methyl alcohol (MeOH) placed in a small volume of limited expansion. The fluid passes through a sequence of phase transformation stages, including supercritical state, fast vaporization and condensation into fine droplets. The dynamics of plasma bubble was explored over a range of electrical parameters and electrodes geometry. The pressure and temperature inside of the test cell was estimated to be above the critical value $P_{cr}$=80bar, $T_{cr}$=513K, based on the electrical measurements. The electron density in plasma sustain in a supercritical fluid, measured using Stark broadening of $H_\alpha$ Balmer series line of hydrogen atoms, is as high as $n_e > 2 \times 10^{19} cm^{-3}$.

## 1. INTRODUCTION

The experimental work is based on the idea of electrical discharge generation in transient supercritical fluid: the working media is stored in the form of a liquid fluid at ambient conditions and is rapidly heated and pressurized by pulsed high-voltage electrical energy and concomitant



*Fig.1. Schematic of phase transformations during transient supercritical plasma generation.*

plasma. In this phase the liquid exhibits a phase change to a supercritical fluid, and then escapes to lower pressure media via fast vaporization with subsequent partial nucleation. The process of phase transformation is roughly illustrated in Fig. 1, where T is what is known as the triple point, and C is the critical point. The exact trajectory of liquid state to supercritical fluid depends on geometry of test cell, fluid thermal properties and electrical power density. In a locked cell the trajectory is linear with a slope $\partial P / \partial T = \beta / k$, where $P$ – pressure, $T$ – temperature, $\beta$ – thermal expansion factor, $k$ – compressibility coefficient. In the presence of ejecting orifice, the pressure becomes lower; but some combination of parameters keeps it higher than of the critical value (points 1 to 2). The reverse process of condensation (points 2 to 3) may be realized by variety of trajectories, all of them result to two-phase composition.

There is a limited bibliography, discussed the electrical discharge appearance and properties in supercritical fluids. Most of experiments are performed in CO2 [1-4] and explore small scale discharges of mm and less inter-electrode gap. In this work the following three issues are discussed: (1) existence of transient supercritical state of fluid; (2) electrical discharge as the method to achieve the supercritical state; (3) dynamics of phase transformation at presence of plasma in a supercritical fluid. The practical benefits are expected at application of transient supercritical state of fluid in liquid fuel injection apparatus [5-8].

## 2. EXPERIMENTAL APPROACH

The test cell consists of a body made of a transparent dielectric material, a discharge channel, an electrode system, a high-voltage power supply and a set of diagnostics. Briefly, a discharge is initiated in the cylindrical test channel using a pair of electrodes. The first electrode ends the channel with diameter *d=1.5-*

Fig.2. Dynamic chart of supercritical injection. Yellow-initial fluid, blue-vapor bubble, red-plasma, violet-supercritical fluid and two-phase fluid.

4mm and length *l=10-25mm*, initially filled with a liquid fuel. The exhaust orifice is drilled in the second electrode on the other end of the channel. This vent may have the same or a smaller diameter than the channel. The scheme is understandable from Fig.2.

The power supply is synchronized with external trigger and produces the maximum voltage up to $U_{max}=15kV$ at current of *I<150A*. Energy deposition is limited to *E=200J/pulse*. The diagnostics include: voltage, current, emission sensors, optical emission spectroscopy, image acquisition camera, line-scan streak camera, schlieren system, sensors of transparency, etc. The last ones are arranged as diode laser sheets traversing the test channel and exhaust jet to confirm achieving of the critical conditions by visual observation of supercritical opalescence of the fluid.

A choice of working fluid is based on following criteria: (1) it should be one of actual fuels; (2) providing the easiest way to supercritical transition; (3) its electrical conductivity should be controllable. In this particular work a mixture of $CH_3OH$ + 10% KOH is utilized for the tests [9]. The specific electrical conductivity is measured as high as *σ=0.05S/m* at low voltage (2volts) and *σ=2S/m* at high voltage (>5kV/cm).

## 3. PLASMA AND FLUID DYNAMICS

Figure 2 imagines dynamic of fluid in test cell: initial stage consists of heating of the liquid by electrical current. If mention a uniform distribution of the electrical parameters along the test cell, the temperature dynamics can be described by equation (1), where *W* is electrical power, *σ* is electrical conductivity, *U* is voltage.
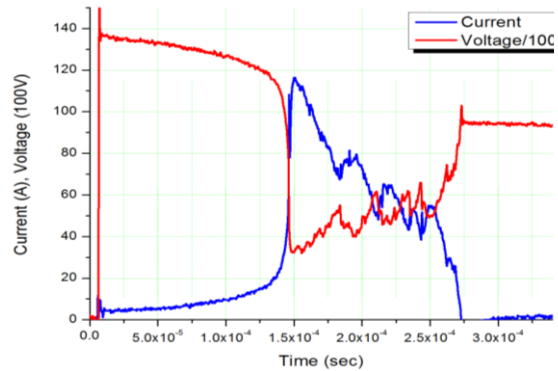


Fig.3. Typical current-voltage oscillograms for l=22mm.

$$\frac{\partial T}{\partial t} = \frac{W}{c \times m} = \frac{\sigma}{c \times \rho} \times \left(\frac{U}{l}\right)^2, \quad (1)$$

In this configuration the temperature first achieves a value where the pressure of saturated vapor is equal to the static pressure at a location nearby one of electrodes. An initial vapor bubble is generated at this point with sequential electrical breakdown of some portion of the test cell, then along the entire cell. The plasma formed pushes the fluid out, increasing the pressure due to electrical discharge power dissipation. The dynamics of the rest of the process in channel with cross-section *A* is determined by the equation (2):

$$m \times \frac{\partial^2 x}{\partial t^2} = p(t) \times A, \quad (2)$$

At some combination of test parameters the supercritical transition is observed in the channel. The oscillograms in Fig.3 show the voltage-current data that allows calculating a corresponding power, energy deposition, fluid resistance, temperature, and pressure. An average temperature achieves the supercritical value already at t<200μs. An installation of extra microelectrodes gives the data on a local value of fluid electrical conductivity: it varies from *σ=2S/m* at initial conditions to *σ=10³S/m* in the phase of high-current plasma.

At least two interfaces were observed inside of the test cell: between plasma and a dark bubble of supercritical fluid, and between the bubble and the initial fluid. Tests were performed to explore dynamics of those interfaces by two techniques:
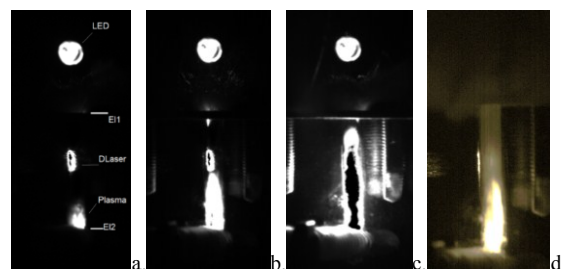


Fig.4. Movement of the bubble's interface along the test channel. Sequence of images, delay 100, 120, 140μs. Exposure 12μs.
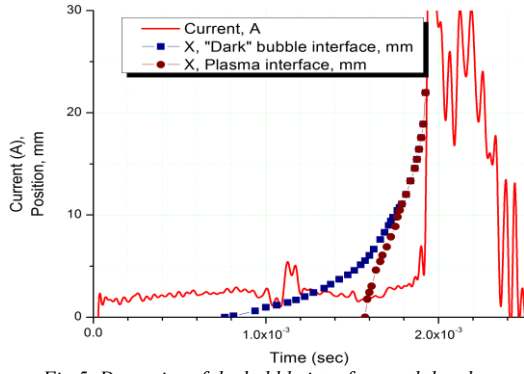
*Fig.5. Dynamics of the bubble interface and the plasma position by line-scan camera.*

sensors of transparency and fast streak camera. In the first case a laser beam crossed the test cell and its intensity is recorded same way as the electrical parameters of the run. The second sensor of transparency (LED) was installed above the test cell to determine the state of what was initially liquid at the exit of the channel. Figure 4 demonstrates the camera images of a slow movement of the plasma interface inside the channel. The last frame in Fig.4d illustrates the picture after main breakdown at t>200µs. It can be seen that the transmission of the LED light through the medium is essentially zero. This phenomenon may be ascribed to nucleation/condensation of the supercritical fluid phase after achieving the supercritical condition. The laser beam is also invisible through the test cell because of the critical opalescence of fluid after reverse transition from the supercritical state.

The dynamics of the bubble interface and the plasma position was inferred from the line-scan camera images. An example is shown in Fig.5 together with a synchronized graph of the electrical current. Based on the equations of the interface movement (2), the pressure in the channel has been calculated. Neglecting evaporation of the fluid interface, such formal approach gives a pressure value of tens of Bar, up to $P_{max}$=90 Bar in particular case of slow mode (plasma initiated at bottom electrode).

## 4. ANALYSIS OF EMISSION SPECTRA

The optical spectra acquisition and processing were performed for preliminary evaluation of the plasma parameters. Princeton Instruments Pixis 256 camera, and spectrograph SpectraPro-300i by Acton Research Corp. were utilized for this purpose; the half-width of spectral instrument functions was less than HWF=0.6nm. The spectrum consists of a strong continuum and a few spectral emission and absorption lines. The most intensive lines are $H_\alpha$ (656nm), atomic

oxygen triplet lines O 777nm (3p5P-3s5S0) and 844nm (3p3P-3s3S0). Potassium absorption lines are easily detectable at 767 and 770nm.

The $H_\alpha$ line of Balmer series is strongly broadened. Generally, three basic mechanisms could be responsible for that: (1) Stark broadening; (2) Van der Waals (VdW) broadening; and (3) Doppler broadening. Stark broadening occurs because of the electrical field perturbation due to interaction with charged particles (mostly electrons):

$$\Delta\lambda_{1/2} = 1.25 \times 10^{-9} \times C \times N_e^{2/3}, \qquad (3)$$

with the electron density $N_e$ and the half width parameter C. This parameter is calculated numerically for different gas temperatures and electron densities. One of the most recent datasets on $H_\alpha$ line is given by Gigosos and also discussed by Griem at high values of electron density [10-11]. In our case, when $H_\alpha$ line is extremely wide (half-width FWHM=10÷40nm), the electron density could be estimated by extrapolation of dataset. Based on relative intensity of atomic oxygen lines and spectral continuum the gas (or fluid) temperature may be considered to be in a range $T_g$=3-5kK. The pressure should be too high to explain the $H_\alpha$ broadening by VdW mechanism in gas. At the same time the supercritical fluid possesses higher density than gaseous media at the same pressure, thus the VdW mechanism might not be neglected at further analysis. The Doppler broadening is definitely less than the first two effects in this particular case. It should be noted that such a wide $H_\alpha$ line was previously observed in underwater electrical discharges and in some other liquids, see [12], for example.

Spectral profiles of $H_\alpha$ line were taken from the plasma plume (zone 1) outside of test cell and from the supercritical plasma in test cell (zone 2). In the latter case the intensity of radiation was order of magnitude higher than outside of the
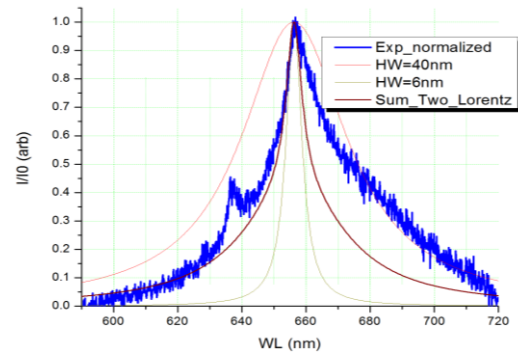


*Fig.6. Spectral fitting of normalized experimental Hα line, taken from zone inside of discharge channel.*

channel. The experimental profiles cannot be satisfactory fitted with a single calculated Lorentz shape. The current hypothesis is as follows: the radiating medium is strongly inhomogeneous and the light emission is collected from two (or a few more) areas with extremely high variation of parameters, particularly – molecular and electron density. They could be vapor phase and supercritical fluid, for example. Figure 6 presents the graphs where the experimental profile is fitted by sum of two Lorentz's profiles with rather dissimilar half width. The formal approach gives the result shown in Table 1.

*Table 1. Electron density due to Hα Stark broadening.*

|        | Low $N_e$, cm$^{-3}$ | High $N_e$, cm$^{-3}$ |
|--------|----------------------|-----------------------|
| Zone 1 | $2.5 \times 10^{17}$ | $6 \times 10^{18}$    |
| Zone 2 | $\sim 10^{18}$       | $> 2 \times 10^{19}$  |

A local value of fluid electrical conductivity was measured as low as $\sigma = 10^2 - 10^3 (\text{Ohm} \times \text{m})^{-1}$ in the phase of high-current plasma. With some assumptions the molecular number density can be estimated based on electrical conductivity and electron density data as follows [13]:

electrical conductivity $\quad \sigma = e \times \mu_e \times n_e = \frac{e^2 \times n_e}{m \times \nu_m}$;

collision frequency $\quad \nu_m = N_m \times A \times \bar{v}_e$;

where A – molecular cross-section, $\bar{v}_e$ – average electrons' velocity. The molecular number density, calculated by this way, is approximately $N_m = 10^{22}$ cm$^{-3}$. The supercritical condition of the fluid should be considered to explain this high value of density.

## 5. SUMMARY

A specific objective of this work was an experimental study of dynamics of media, phase transformation, and measurements of plasma parameters during high-voltage electric discharge generation in transient supercritical fluid. Calculations based on the measured electrical parameters of fluid and on incompressible fluid model indicate that, for some combination of test parameters, the pressure (*P> 80Bar*) and the temperature (*T>513K*) in the test cell exceed the characteristic values for supercritical condition. The electron density Ne$>2.5 \times 10^{19}$ cm$^{-3}$ in plasma was measured by Stark broadening of hydrogen line H$_\alpha$ (656nm) of Balmer series. To reconcile these data with the electrical conductivity measured in the test cell, the molecular number density must be higher than $N_m = 10^{22} cm^{-3}$. This suggests a conclusion that the technique applied allows transition of liquid media to the state of supercritical fluid, with subsequent formation of "supercritical" plasma.

## REFERENCES

[1] M Goto, M Sasaki, T Kiyan, et all, "Reaction in Plasma Generated in Supercritical Carbon Dioxide", Journal of Physics: Conference Series 121 (2008) 082009

[2] T. Ito, K. Terashima, "Generation of micrometer-scale discharge in a supercritical fluid environment", Appl. Phys. Lett. 80, 2854 (2002)

[3] A. Kawashima, H. Toyota, S. Nomura, et all, "27.12 MHz plasma generation in supercritical carbon dioxide," J. Appl. Phys., vol. 101, no. 9, pp. 093, May 2007

[4] E. H. Lock, A. V. Saveliev, L. A. Kennedy "Influence of Electrode Characteristics on DC Point-to-Plane Breakdown in High-Pressure Gaseous and Supercritical Carbon Dioxide", IEEE Transactions On Plasma Science, Vol. 37, No. 6, June 2009.

[5] T. J. Bruno and J. F. Ely, Supercritical Fluid Technology: Review in Modern Theory and Applications, CRC Press, 1991

[6] Edwards, T., "USAF Supercritical Hydrocarbon Fuels Interests," AIAA Paper 93-0807, 1993.

[7] A. Roy, C. Segal, and C. Joly "Spreading Angle and Core Length of Supercritical Jets", AIAA Journal, Vol. 51, No. 8 (2013), pp. 2009-2014.

[8] De Boer, C., Bonar, G., Sasaki, S., and Shetty, S., "Application of Supercritical Gasoline Injection to a Direct Injection Spark Ignition Engine for Particulate Reduction," SAE Technical Paper 2013-01-0257, 2013

[9] R. D. Goodwin, "Methanol Thermodynamic Properties from 176 to 673K at Pressure to 700Bar", J. Phys. Chem. Ref. Data, Vol.16, No 4, 1987

[10] M. Gigososy, V. Cardenosoz, "New plasma diagnosis tables of hydrogen Stark broadening including ion dynamics", J. Phys. B: At. Mol. Opt. Phys. 29 (1996) 4795–4838.

[11] H. R. Griem, "Stark Broadening of the Hydrogen Balmer-α Line in Low High Density Plasmas", Contrib. Plasma Phys. 40 (2000), pp.46-56

[12] P. Bruggeman, T. Verreycken, M. Gonzalez, et all, "Optical emission spectroscopy as a diagnostic for plasmas in liquids: opportunities and pitfalls", J. Phys. D: Appl. Phys. 43 (2010) 124005 (8pp)

[13] Yu. P. Raizer "Gas Discharge Physics", Springer, Berlin, New York, 1997